Stability and Active Power Sharing in Droop Controlled Inverter Interfaced Microgrids: Effect of Clock Mismatches

Ramachandra Rao Kolluri [a,c], Iven Mareels [a], Tansu Alpcan [a], Marcus Brazil [a], Julian de Hoog [b,c] and Doreen Thomas [b].

[a] *Department of Electrical and Electronic Engineering, The University of Melbourne, Parkville, VIC 3010 Australia*

[b] *Department of Mechnical Engineering, The University of Melbourne, Parkville, VIC 3010 Australia*

[c] *IBM Research Australia, Victoria, Australia*

Abstract

Stability and power sharing properties of droop controlled inverter-based microgrid systems depend on various design factors. Little explored is the effect of component mismatches and parameters drifts on the stability, steady state behaviour and power sharing properties of these systems. In this paper, the behaviour of frequency droop controlled inverter based microgrid systems in the presence of non-identical clocks is analysed. It is shown that power sharing between converters in a microgrid can be sensitive to clock mismatches. Our proposal shows that a coordination control that uses sparse inter-node communications is useful in ensuring desired active power sharing. Conditions are derived to ensure stability in the presence of the proposed controller and simulation results are presented.

Key words: AC microgrids, active power sharing, autonomous microgrid, distributed control, droop control, microgrids, power system reliability, power system stability, smart grids and synchronization.

1 Introduction

Integration of renewable energy has been proposed as a feasible technique to elude the increasing electricity prices and simultaneously alleviate carbon emissions. Most often, the renewable energy sources are spatially distributed making domestic consumption, through traditional radial power flow, a lossy system. Microgrids and storage, therefore, appear as natural extensions to this decentralization of renewable energy generation. Traditional generation (using rotating machines) is well understood and its availability is deemed to be very important to easily maintain the voltage and frequency levels. Despite the fact that microgrids are envisioned as exciting opportunities, the majority of the sources within them are power electronic converter (inverter) based. There are some technical challenges that have to be addressed before there can be large scale deployment of modern microgrids.

Parallel operation and power sharing between inverter based sources through frequency droop control was first proposed in [1]. Drawing motivation from the operation of synchronous generators, frequency droop controlled inverters measure their real and reactive power output and accordingly modify their frequency and voltage, respectively. Certain design criteria are used to ensure proportional power sharing between inverters in such systems. Various aspects of frequency droop controlled microgrid systems have been discussed in [2, 3].

Frequency/clock mismatches affect frequency droop controlled systems. The majority of the work in inverter interfaced microgrids based on droop control focuses on the stability and efficiency of these systems under some assumptions. A few papers [4, 5] have commented on the significance of computational delays, numerical errors and parameter uncertainties and acknowledged their effect on the power sharing between droop controlled systems. In [4] a qualitative analysis is performed to demonstrate the contribution of these component mismatches to inaccuracy in power sharing (specifically those arising from voltage mismatches when real power - voltage droop control is used). A robust voltage controller is then proposed to mitigate these effects. Simulation results in [5] show that unequal response times between inverters may lead to network instability. However, neither work discusses the affect of parameter mismatches on the stability of the overall system from a qualitative

[1] Corresponding author email: *rkolluri@au1.ibm.com.* This work has been partly funded by a Linkage Grant supported by the Australian Research Council, Better Place Australia and Senergy Australia.

perspective, particularly when the mismatches are in the form of frequency. Some authors have acknowledged the issues arising from these mismatches. Papers [4, 6] showed some simulation results illustrating the issues. In [7] the mismatches arising from clock drifts are well addressed but their assumption on line resistance and small drifts are considered and questioned in the present work. While it is possible to have frequency mismatches arising from various scenarios like, crystal inaccuracies, inaccurate pre-synchronization of inverter interconnection [6] and so on, an assumption that the clock is very stable and accurate pervades the microgrid literature.

1.1 Contribution

In this work, the effectiveness of classical frequency droop control is revisited in the context of clock drifts. The main contributions of this work are twofold. Firstly, small frequency variations are natural in inverters and it is shown that their mere presence will disturb the power distribution equilibrium and may potentially impact stability. Inspired by consensus-based frequency restoration [2] and consensus-based droop control techniques [8], a modified version of droop control is presented to restore the desired power distribution equilibrium. Secondly, taking our control technique into account, we establish stability for a constant impedance load based microgrid. Moreover, the proposed control technique is supplementary to traditional frequency droop control, unlike some works, for example [9], thereby retaining the stability and power sharing properties of the former under communication outages. We provide stability conditions for a Kron reduced network using our proposed controller through Lyapunov's indirect method. We show that there are multiple zero eigenvalues for the linearized state transition matrix and therefore use dimensionality reduction to emphasize that the zeros arise from redundancy in the controller implementation. Our proposal provides improved power sharing performance for smaller droop coefficients also thereby reducing frequency deviation. This will in-turn assist in improving model accuracy. Simulation results that demonstrate the efficacy of the proposed controller are also presented.

1.2 Preliminaries and Notation

In an n inverter (node) system we define the n-dimensional column vector $x = col(x_i) = [x_1, x_2, \ldots, x_n]^T$ where $(\cdot)^T$ represents a transpose function. Let $diag(x_i)$ be a $(n \times n)$-dimensional diagonal matrix with x_i in the i^{th} row and i^{th} column and 0 elsewhere. The $(n \times n)$-dimensional identity matrix is given by $\mathbf{I}_n = diag(1)$. The matrix $1_{n\times n}$ is a $(n \times n)$-dimensional matrix with all elements equal to 1. If $\underline{y} = a + jb$ is a complex number with $j = \sqrt{-1}$, then the real part is given by $\Re\{\underline{y}\} = a$ and the imaginary part is given by $\Im\{\underline{y}\} = b$. The notation $(\cdot)^*$ denotes complex conjugate of a complex number. A communication network is represented as a connected graph $\mathbf{G}_c = (\mathbf{V}_c, \mathbf{E}_c)$, where $\mathbf{V}_c$ is the set of nodes and $\mathbf{E}_c$ is the set of edges which represent the communication links between nodes. We define the communication degree matrix $\mathbf{D}_c := diag(\deg(i))$, where $\deg(i)$ is the number of communication links connected to the i^{th} node. Adjacency matrix $\mathbf{A}_c$ represents the connections between nodes in the communication graph with $a_{ij} = a_{ji} = 1$ if the nodes i and j are connected, and $a_{ij} = a_{ji} = 0$ otherwise. Self loops are avoided, meaning $a_{ii} = 0$ for any node i. We denote the communication graph Laplacian $\mathbf{L}_c = \mathbf{D}_c - \mathbf{A}_c$. The vector 1_n is basis of the kernel of $\mathbf{L}_c$ i.e., for any vector $c = \theta 1_n, \theta \in \mathbb{R} \setminus \{0\}$ we have $\mathbf{L}_c c = 0_n$ and since the matrix is symmetric we also have $c^T \mathbf{L}_c = 0_n^T$. Its eigenvalues $\{\lambda_{c,1}, \lambda_{c,2}, \ldots \lambda_{c,n}\}$ obey the relationship [10]: $0 = \lambda_{c,1} < \lambda_{c,2} \leq \ldots \lambda_{c,n}$.

2 System Set-up

2.1 Modelling clock drifts

To facilitate an analysis that considers the clock drift effect, we denote the voltage at each inverter in terms of a common reference time t. The common time reference, in most cases, is fictitious and not available for measurement. We can represent the local time t_i with respect to a reference time t as shown in (1) [7]:

$$t_i = t\,(1 + \epsilon_i)\,, \tag{1}$$

where ϵ_i is the time invariant drift of the local clock with respect to the reference clock. As emphasized earlier, this drift is natural in clock based systems and must be included for a complete analysis. As in [2] we model the i^{th} inverter as an averaged voltage source :

$$v_i(t) = V_i \cos(\omega t_i + \delta_i) = V_i \cos(\omega_i t + \delta_i),$$

where V_i is the voltage amplitude; $\omega_i = \omega + \eta_i$ is the new frequency with $\eta_i = \epsilon_i \omega$ and ω is the set-point frequency. Here η_i is the drift in the frequency at the inverter arising from individual non-ideal clocks. Since the literature does not suggest how fast ϵ_i varies with time we have not considered a time varying drift. Using commonly reported values for the clock drift, ϵ_i, a frequency drift in the order of 0.03 Hz (for reference frequencies around 50 or 60 Hz) is to be expected, as seen in Table 1. The table lists $\eta = \epsilon\omega$ as well as the corresponding per unit time scale variable $\gamma = 1/(1 + \epsilon)$.

Therefore, an approximate steady state drift $|\epsilon_i|$ of the order of 10^{-3}p.u to 10^{-6}p.u can be subsequently derived. It should be noted that the local integration process at each inverter is affected by the clock drifts. Using (1) we can redefine the local integrator / differentiator as [7]:

$$\frac{d(\cdot)}{dt_i} = \gamma_i \frac{d(\cdot)}{dt} := \gamma_i \dot{(\cdot)},$$

Table 1
Drifts in commercial inverters

Reference	$\lvert\eta\rvert$(Hz)	γ
[11]	0.05	1 ± 0.001
[12]	0.025	1 ± 0.0005
[13]	0.05	1 ± 0.001
[14]	0.06	1 ± 0.001
[15]	0.025	1 ± 0.0005

where $\gamma_i = (1+\epsilon_i)^{-1}$. Observe that any local state will be affected by the clock deviation. Hence, the dynamical system model must take this into account.

2.2 Droop control and power sharing

According to [1], the amount of real power flowing between two nodes can be controlled by altering the phase angle δ between them. This forms the basis of so-called *frequency droop* controller as shown in (2).

$$\omega_i = \gamma_i \dot{\delta}_i = \omega^* - m_i(P_i - P_i^*), \tag{2}$$

where m_i is the droop coefficient, P_i is the active power output and $(\cdot)^*$ represents rated values of the i^{th} inverter. It is known that active power sharing in frequency droop controlled inverter based microgrids is achieved by designing the droop coefficients according to a power sharing criteria: $m_i P_i^* = m_j P_j^*,\ \forall i,j \leq n$ [1]. Deviation in power sharing between inverters i and j that results from clock drifts and zero rated powers can be quantified as:

$$\omega^* \left(\frac{1}{\gamma_i} - \frac{1}{\gamma_j}\right) = \frac{m_i P_i^s}{\gamma_i} - \frac{m_j P_j^s}{\gamma_j}$$

The values P_i^s and P_j^s are steady state powers and are implicitly dependent on system loading. To summarize, there are two variables that largely impact power sharing. First, the droop coefficient, m_i - it can be made large subject to large frequency deviations and oscillatory transient response. It follows that we must consider the clock drift in designing the droop control. But, the clock drifts are unknown and very hard to measure. Second, the (relative) clock drifts, γ_i - which are hard to measure as well. Therefore, it is very useful to find a method that ensures proper power sharing and stability for arbitrarily small droop coefficients even in the presence of unknown clock mismatches without needing to measure extra variables. Another major advantage is that the network resilience for frequency dependent loads will then automatically be ensured without any extra control owing to the small frequency deviation from small droop coefficients. In an energy and power limited scenario like a microgrid, proportional power sharing design will consequently ensure operation longevity.

2.3 Assumptions

The following is assumed in the remainder of this paper:

- there are n inverters connected to the microgrid and each is interfaced via controllable power electronics and has a DC link (for example, a storage unit) that can allow bi-directional power flow. Since optimal sizing of the battery is not the focus of this work, the battery here can also be considered as an infinite DC bus;
- the output voltage amplitude of the inverter is held at a constant value. In other words, the analysis carried out here does not consider the dynamics of voltage amplitude and any voltage amplitude control loops such as, reactive power voltage droop, are neglected or considered to be at the design equilibrium;
- the line resistances, although present, are assumed to be small as per the traditional frequency droop controller assumptions. In this regard, if this was not the case, a virtual impedance emulation technique can be used to ensure this assumption is valid; and
- the microgrid network is analysed based on Kron reduction using an assumption that the loads are constant impedance type. In such a network, Y_{ii} is the self-admittance and Y_{ik} is the admittance between inverters i and k. $Y_{ik} = G_{ik} + jB_{ik} = |Y_{ik}|\angle\phi_{ik}$ where G is the conductance, B is the susceptance at the system nominal frequency and θ is the admittance angle. It is recommend that the reader refers to [16] for discussion on implications that arise from different load types.

2.4 Modified frequency droop

Considering the clock mismatches, dynamics of the phase angle of the i^{th} inverter in a frequency droop controlled microgrid are represented by (2) with $\delta_i \in \mod 2\pi$. The feedback power P_i is a local variable measured at the i^{th} inverter output; ω^* and P_i^* are the global and local constants by design, respectively. Since the feedback is purely local, it can be understood that there is no requirement for additional communications to implement the simple frequency droop controller on an inverter [17]. The local feedback variable is the measured power, P_i and its measurement often involves a filter stage. This filter stage introduces first-order dynamics into the system as follows:

$$\tau_i \gamma_i \dot{P}_i = -P_i + p_i, \tag{3}$$

where τ_i is the filter time constant and p_i is the actual output power of the i^{th} inverter which is given by the power flow equation [18]:

$$p_i = G_{ii}V_i^2 + \sum_{k\neq i} |Y_{ik}|V_iV_k \sin(\delta_i - \delta_k + \phi_{ik}).$$

To counter-act the power sharing mismatch introduced by clock drifts a *modified frequency droop* control scheme is proposed in this paper. The proposal makes use of inter-node communications to include an integral control action that enables inverters to share power according to a sharing criterion even in the presence of clock uncertainties / mismatches. This kind of communication architecture is most commonly used in power systems for secondary control (see [19] for instance).

The integral term z_i is defined as:

$$\gamma_i \dot{z}_i = k_i \sum_{j \in \mathbf{N}_i} (m_i P_i - m_j P_j), \tag{4}$$

where $k_i > 0$ is the local integral control gain and $\mathbf{N}_i$ represents the set of inverters communicating with the i^{th} inverter. This integral control term is added as negative feedback to the frequency droop controller as:

$$\gamma_i \dot{\delta}_i = \omega^* - m_i P_i + m_i P_i^* - z_i. \tag{5}$$

The integral terms have zero initial value and are disconnected when communication outages occur (for example, $m_j P_j = 0$) to retain system stability as in simple droop control. The importance of this will be made clear in the later parts of the paper. It is apparent that there are no extra measurements required to perform the integral control and the communications associated are distributed. Thus, the complexity of implementation is not significantly increased and the system robustness / modularity requirements are still well-preserved. The ability of this control technique to ensure proper power sharing and stability is discussed next.

3 Stability Analysis

3.1 Stability under consensus control

Define vectors / matrices: $1_n := col(1)$, $0_n := col(0)$, $\mathbf{P}_m := col(P_i)$, $\mathbf{P}^* := col(P_i^*)$, $\mathbf{P}_a := col(p_i)$, $\boldsymbol{\delta} := col(\boldsymbol{\delta}_i)$, $\mathbf{V} := col(V_i)$, $\mathbf{Z} := col(z_i)$, $0_{n\times n} := diag(0)$, $\mathbf{M} := diag(m_i)$, $\boldsymbol{\Gamma} := diag(\gamma_i)$, $\mathbf{K} := diag(k_i)$ and $\mathbf{T} := diag(\tau_{p,i})$.

From equations (3), (4), (5) and using the vector notation introduced earlier, the microgrid dynamics can be represented by:

$$\boldsymbol{\Gamma}\dot{\boldsymbol{\delta}} = \omega^* 1_n - \mathbf{M}(\mathbf{P}_m - \mathbf{P}^*) - \mathbf{Z}, \tag{6}$$

$$\boldsymbol{\Gamma}\mathbf{T}\dot{\mathbf{P}}_m = \mathbf{P}_a - \mathbf{P}_m, \tag{7}$$

$$\boldsymbol{\Gamma}\dot{\mathbf{Z}} = \mathbf{K}\mathbf{L}_c\mathbf{M}\mathbf{P}_m. \tag{8}$$

Assumption 1 *Assume that there exists a steady-state in the system (6-8) and the equilibrium vectors (a manifold of equilibria) are denoted by $\boldsymbol{\delta}^s$, $\mathbf{V}^s$, $\mathbf{P}_m^s$ and $\mathbf{Z}^s$. The deviation of state vectors from their respective equilibria is denoted by the deviation vectors $\bar{\boldsymbol{\delta}}$, $\bar{\mathbf{V}}$, $\bar{\mathbf{P}}_m$ and $\bar{\mathbf{Z}}$. Also assume that the equilibrium phase angle vector is in the n-torus, $\boldsymbol{\delta}^s \in \mathbb{T}^n : \{-\pi, \pi\}$ s.t $\frac{\pi}{2} > |\delta_i^s - \delta_k^s + \phi_{ik}|$ $i, k = 1, \ldots, n$. The equilibrium phase angle vector represent synchronous (phase-locked) motion relative to a synchronous network frequency, ω^s.*

Linearizing the non-linear power flow term $\mathbf{P}_a$ in the ordinary differential equation (7) with respect to $\boldsymbol{\delta}$ at equilibrium vectors $\boldsymbol{\delta}^s, \mathbf{V}^s$ yields a linear dynamical system which is much easier to analyse. This linearization is defined as:

$$\mathbf{L}_n := \frac{\partial \mathbf{P}_a}{\partial \boldsymbol{\delta}}_{|\boldsymbol{\delta}^s, \mathbf{V}^s} = \begin{bmatrix} \frac{\partial p_1}{\partial \delta_1} & \cdots & \frac{\partial p_1}{\partial \delta_n} \\ \vdots & \ddots & \vdots \\ \frac{\partial p_n}{\partial \delta_1} & \cdots & \frac{\partial p_n}{\partial \delta_n} \end{bmatrix}_{|\boldsymbol{\delta}^s, \mathbf{V}^s} .$$

The matrix $\mathbf{L}_n$ is a network Laplacian with positive diagonal (l_{ii}) and non-positive off-diagonal elements (l_{ik}) as shown in (9) and (10), respectively. The entries of the network Laplacian obey condition (11).

$$l_{ii} = \sum_{i \neq k} a_{ik} \cos(\delta_i^s - \delta_k^s + \phi_{ik}), \tag{9}$$

$$l_{ik} = -a_{ik} \cos(\delta_i^s - \delta_k^s + \phi_{ik}), \tag{10}$$

$$l_{ii} = -\sum_{k=1, k\neq i}^{n} l_{ik}, \tag{11}$$

where $a_{ik} = V_i^s V_k^s |Y_{ik}|$. The matrix $\mathbf{L}_n$ has a simple eigenvalue that is zero and the remaining eigenvalues have a positive real part [20]. It is also important to note that the vector 1_n forms the basis of $\mathbf{L}_n$'s kernel i.e., for any vector $w = \beta 1_n, \beta \in \mathbb{R} \setminus \{0\}$ we have $\mathbf{L}_n w = 0_n$.

Assumption 2 *We assume that the power measurement low-pass filter coefficients of each inverter system are identical, i.e., $\mathbf{T}^{-1} = f\mathbf{I}_n$. We also assume that the integral control gains are identical i.e., $\mathbf{K} = k\mathbf{I}_n$.*

Following linearization and embedding the assumption 1 and assumption 2 into (6-8) yields the closed loop microgrid model that reflects the dynamics around the manifold of equilibria. It is given by,

$$(\mathbf{I}_3 \otimes \boldsymbol{\Gamma}) \begin{bmatrix} \dot{\bar{\boldsymbol{\delta}}} \\ \dot{\bar{\mathbf{P}}}_m \\ \dot{\bar{\mathbf{Z}}} \end{bmatrix} = \underbrace{\begin{bmatrix} 0_{n\times n} & -\mathbf{M} & -\mathbf{I}_n \\ f\mathbf{L}_n & -f\mathbf{I}_n & 0_{n\times n} \\ 0_{n\times n} & k\mathbf{L}_c\mathbf{M} & 0_{n\times n} \end{bmatrix}}_{:=\mathbf{F}} \begin{bmatrix} \bar{\boldsymbol{\delta}} \\ \bar{\mathbf{P}}_m \\ \bar{\mathbf{Z}} \end{bmatrix}, \tag{12}$$

where $\otimes$ denotes Kronecker product. The eigenvalues of

state transition matrix $\mathbf{F}$ defined in (12) will predominantly determine the stability of the modified frequency droop controller based microgrid around the manifold of equilibria.

Theorem 3 (Eigenvalues under consensus control) *Suppose that σ_i is the i^{th} the eigenvalue of the matrix product $\mathbf{ML}_n$ and similarly, μ_i is the i^{th} eigenvalue of the matrix product $\mathbf{L}_c\mathbf{ML}_n$. Consequently, the matrix $\mathbf{F}$ in (12) possesses $(3n-2)$ eigenvalues that have a negative real part for a choice of k given by:*

$$k < f \min_{>0} \Re\left(\frac{\sigma_i}{\mu_i}\right). \tag{13}$$

In stable steady state proportional power sharing is also achieved amongst sources in the microgrid.

Proof: We utilize the arguments explored in [21, 19] for our proof. Firstly, in stable steady state, the integral controller ensures that the power shared between inverters meets the prescribed power sharing criterion. Recall that the matrix $\mathbf{L}_c$ is the communication Laplacian with positive eigenvalues along with one zero eigenvalue. Consequently, in steady state we have,

$$0_n = k\mathbf{L}_c\mathbf{MP}^s_m \iff \mathbf{MP}^s_m = \nu 1_n \iff m_iP^s_i = m_jP^s_j,$$

where $\nu \in \mathbb{R} \setminus \{0\}$ is a constant for all the inverters $i, j \in n$ and is based on the initial conditions and network aggregate load. To prove the second part of our claim, we operate on the linear state transition matrix $\mathbf{F}$. Consider the characteristic equation of $\mathbf{F}$ given by,

$$\det(\lambda_{\mathbf{F}}\mathbf{I}_{3n} - \mathbf{F}) = \begin{vmatrix} \lambda_{\mathbf{F}}\mathbf{I}_n & \mathbf{M} & \mathbf{I}_n \\ -f\mathbf{L}_n & (\lambda_{\mathbf{F}}+f)\mathbf{I}_n & 0_{n\times n} \\ 0_{n\times n} & -k\mathbf{L}_c\mathbf{M} & \lambda_{\mathbf{F}}\mathbf{I}_n \end{vmatrix}.$$

Using identities from [22], we have

$$\det(\lambda_{\mathbf{F}}\mathbf{I}_{3n} - \mathbf{F}) = \det(\mathbf{Q}(\lambda_{\mathbf{F}})),$$

where

$$\mathbf{Q}(\lambda_{\mathbf{F}}) = \lambda^3_{\mathbf{F}} + f\lambda^2_{\mathbf{F}} + f\lambda_{\mathbf{F}}\mathbf{ML}_n + fk\mathbf{L}_c\mathbf{ML}_n. \tag{14}$$

To compute the eigenvalues, let $v \in \mathbb{C}^n$ be any vector with $v^*v = 1$. Left multiplying the characteristic polynomial (14) by v_i^* and right multiplying by v_i, $\forall i = 1, \ldots, n$, yields

$$\Phi_i\lambda^3_{\mathbf{F},i} + \Pi_i\lambda^2_{\mathbf{F},i} + \Psi_i\lambda_{\mathbf{F},i} + \Sigma_i = 0, \tag{15}$$

where $\Phi_i = 1$, $\Pi_i = f$, $\Psi_i = fv_i^*(\mathbf{ML}_n)v_i$ and $\Sigma_i = fkv_i^*(\mathbf{L}_c\mathbf{ML}_n)v_i$, $\forall i = 1, \ldots, n$.

- When $v_1 = \psi 1_n$, $\psi \in \mathbb{R} \setminus \{0\}$ we have $v_1^*\mathbf{ML}_nv_1 = 0$ and $v_1^*\mathbf{L}_c\mathbf{ML}_nv_1 = 0$, by definition. Consequently (15) becomes:

  $$\lambda^2_{\mathbf{F},1}(\Phi_1\lambda_{\mathbf{F},1} + \Pi_1) = 0.$$

  This implies that $\lambda_{\mathbf{F},1_{1,2}} = 0$ are the two zero eigenvalues of the matrix $\mathbf{F}$. The third eigenvalue associated with this eigenvector ($\lambda_{\mathbf{F},1_3} = \dfrac{-\Pi_1}{\Phi_1} = -f$) is always negative, by definition.
- The remaining $(3n-3)$ eigenvalues ($\lambda_{\mathbf{F},i_{1,2,3}}$, $i = 2, \ldots, n$) will have a negative real part if and only if

  $$\Phi_i\Sigma_i < \Pi_i\Psi_i, \quad i = 2, \ldots, n. \tag{16}$$

  We can ensure (16) is always satisfied by imposing bounds on k. We know

  $$\begin{aligned} \Pi_i\Psi_i &= f^2v_i^*\mathbf{ML}_nv_i, \quad i = 2, \ldots, n, \\ &= f^2\sigma_i, \end{aligned} \tag{17}$$

  from the theorem statement. Based on properties of matrices $\mathbf{L}_n$, $\mathbf{L}_c$ and $\mathbf{M}$ we observe that only the vector 1_n forms the basis of the kernel of $\mathbf{L}_c\mathbf{ML}_n$. We remark that this product term has only one zero eigenvalue since $\mathbf{L}_n$ cannot map any non-zero vector to the basis of its kernel owing to orthogonality of kernel and image spaces [23]. Therefore, from the theorem statement we also have

  $$\begin{aligned} \Phi_i\Sigma_i &= fkv_i^*\mathbf{L}_c\mathbf{ML}_nv_i, \quad i = 2, \ldots, n, \\ &= fk\mu_i. \end{aligned} \tag{18}$$

  Using (17) and (18), we observe that the choice of k according to (13) ensures that (16) holds and will consequently result in remaining eigenvalues that only have a negative real part. □

Corollary 4 *The stability condition for the matrix $(\mathbf{I}_3 \otimes \mathbf{\Gamma})^{-1}\mathbf{F}$, i.e., the entire system (12) is*

$$k < f \min_{>0} \Re\left(\frac{\bar{\sigma}_i}{\bar{\mu}_i}\right). \tag{19}$$

where $\bar{\sigma}_i$ is the ith eigenvalue of $\mathbf{\Gamma}^{-4}\mathbf{M}\mathbf{\Gamma}^{-2}\mathbf{L}_n$ and μ_i is the ith eigenvalue of $\mathbf{\Gamma}^{-5}\mathbf{L}_c\mathbf{M}\mathbf{\Gamma}^{-1}\mathbf{L}_n$.

Proof: Following Theorem 3, observe that the matrix $\mathbf{\Gamma}$ is an invertible diagonal matrix with positive entries that are all very close to unity. Making analogous modifications for $(\mathbf{I}_3 \otimes \mathbf{\Gamma})^{-1}\mathbf{F}$ it can be shown that (19) will result in $(3n-2)$ stable eigenvalues for system (12). For most practical purposes and moreover, since there is a lack of information, $\mathbf{\Gamma}$ can be replaced by an identity matrix and design k sufficiently smaller than the condition (13) to guarantee stability of the system in the presence of clock drifts. However, the condition (19) makes the dependency of the eigenvalues on $\mathbf{\Gamma}$ explicit. □

3.2 Eliminating redundancy

It has been shown that the linearized closed-loop system (12) has two zero eigenvalues. It can also be shown that the dynamics of the center manifold can be factored out, thus proving exponential stability. For this purpose a new state vector, $\mathbf{y}$ is defined by utilizing the translational invariance in phase angle, $\boldsymbol{\delta}$. The elements of $\mathbf{y}$ are given in (20). Redefine z_1 as shown in (21) by imposing zero initial conditions on all the integral control variables, z_i, i.e., $z_i(t_{=0}) = 0$ and based on the fact that vector 1_n is the basis of the kernel of $\mathbf{L}_c$ (by which $\mathbf{Z}$ is defined) and Assumption 2.

$$y_\ell = \delta_\ell - \delta_1, \quad \forall \ell = 2, \ldots, n \tag{20}$$

$$z_1 = -\frac{1}{\gamma_1}\sum_{\ell=2}^{n} \gamma_\ell z_\ell, \quad \forall \ell = 2, \ldots, n \tag{21}$$

The evolution of the new state, y_ℓ can be written as:

$$\begin{aligned}\gamma_\ell \dot{y}_\ell &= \gamma_\ell \dot{\delta}_\ell - \gamma_\ell \dot{\delta}_1 \\ &= \omega^* - m_\ell(P_\ell - P_\ell^*) - z_\ell - \frac{\gamma_\ell}{\gamma_1^2}\sum_{\ell} \gamma_\ell z_\ell \\ &\qquad + \frac{\gamma_\ell}{\gamma_1}(m_1(P_1 - P_1^*) - \omega^*).\end{aligned}$$

Define:

$$\begin{aligned}&\mathbf{Z}_{new} := col(z_2, \cdots, z_n), \quad \mathbf{R}_0 := \left[\, 0_{(n-1)\times 1} \,\middle|\, \mathbf{I}_{(n-1)} \,\right], \\ &\boldsymbol{\gamma}_{new} := col(\gamma_2, \cdots, \gamma_n), \quad \boldsymbol{\Gamma}_{new} := diag(\boldsymbol{\gamma}_{new}), \\ &\mathbf{V} := \left[\, \frac{m_1}{\gamma_1}\boldsymbol{\gamma}_{new} \,\middle|\, -\mathbf{R}_0\mathbf{M}\mathbf{R}_0^T \,\right] \text{ and } \mathbf{L}_n\mathbf{R}_0^T = \frac{\partial \mathbf{P}_a}{\partial \mathbf{y}}_{|\mathbf{y}^s, \mathbf{V}^s}.\end{aligned}$$

We also define $\bar{\mathbf{y}} = \mathbf{y} - \mathbf{y}^s$ and $\bar{\mathbf{Z}}_{new} = \mathbf{Z}_{new} - \mathbf{Z}_{new}^s$, where $\mathbf{y}^s$ and $\mathbf{Z}_{new}^s$ are the equilibrium vector associated with $\mathbf{y}$ and $\mathbf{Z}_{new}$, respectively. Based on the new definitions, the linearized closed loop system can be given by

$$\mathbf{U}\begin{bmatrix}\dot{\bar{\mathbf{y}}} \\ \dot{\bar{\mathbf{P}}}_m \\ \dot{\bar{\mathbf{Z}}}_{new}\end{bmatrix} = \underbrace{\left[\begin{array}{c|c|c} 0_{(n-1)\times(n-1)} & \mathbf{V} & \frac{-\boldsymbol{\gamma}_{new}\boldsymbol{\gamma}'_{new}}{\gamma_1^2} - \mathbf{I}_{(n-1)} \\ \hline \mathbf{L}_n\mathbf{R}_0^T & -f\mathbf{I}_n & 0_{n\times(n-1)} \\ \hline 0_{(n-1)\times(n-1)} & k\mathbf{R}_0\mathbf{L}_c\mathbf{M} & 0_{(n-1)\times(n-1)} \end{array}\right]}_{:=\mathbf{F}_{new}} \begin{bmatrix}\bar{\mathbf{y}} \\ \bar{\mathbf{P}}_m \\ \bar{\mathbf{Z}}_{new}\end{bmatrix},$$

where $\mathbf{U} = diag(\boldsymbol{\Gamma}_{new}, \boldsymbol{\Gamma}, \boldsymbol{\Gamma}_{new})$. The matrices $\mathbf{F}$ and $\mathbf{F}_{new}$ represent the same modified frequency droop controlled system, albeit the latter having the redundant variables removed. It can be proved that this system is devoid of the zero eigenvalues by showing $\mathbf{F}_{new}$ has a non-zero determinant. The determinant of $\mathbf{F}_{new}$ can be calculated using [22]:

$$\det(\mathbf{F}_{new}) = \left|\frac{-\boldsymbol{\gamma}_{new}\boldsymbol{\gamma}'_{new}}{\gamma_1^2} - \mathbf{I}_{(n-1)}\right| \left|\begin{array}{c|c} \mathbf{L}_n\mathbf{R}_0^T & -f\mathbf{I}_n \\ \hline 0_{(n-1)\times(n-1)} & k\mathbf{R}_0\mathbf{L}_c\mathbf{M} \end{array}\right|$$

Since k and f are greater than zero by definition, we have:

$$\det(\mathbf{F}_{new}) \propto \left|\frac{-\boldsymbol{\gamma}_{new}\boldsymbol{\gamma}'_{new}}{\gamma_1^2} - \mathbf{I}_{(n-1)}\right| \left|\mathbf{R}_0\mathbf{L}_c\mathbf{M}\mathbf{L}_n\mathbf{R}_0^T\right| \tag{22}$$

By induction, we can show that the magnitude of the first term in (22) is $1+(\gamma_2^2+\ldots\gamma_n^2)/\gamma_1^2$ which is monotonously increasing with n and always greater than one for values of γ considered in this paper. The last term in (22) is obtained using Cauchy Binet's determinant formula [23]. Since the basis of the kernels of $\mathbf{L}_n$ and $\mathbf{L}_c$ cannot be mapped through the matrices $\mathbf{R}_0^T$ and $\mathbf{R}_0$, respectively, we can say that the determinant of this term is never zero. The remaining is a product of non-zero values proving $\det \mathbf{F}_{new} \neq 0$.

Remark 5 *We have demonstrated that the manifold of equilibria is locally attractive, and by construction of equilibria we can prove that proportional power sharing can be achieved on the equilibrium points. The zero initial condition of the integral control variables is not detrimental, but is a use case, as the actual distribution of the phase angle vectors depends on the initial condition and any other initial condition will satisfy the arguments explored but may require work to prove.*

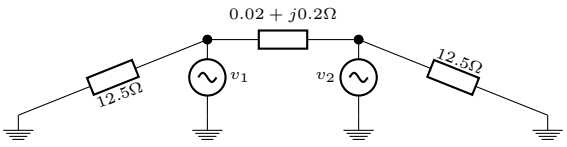

Fig. 1. Kron reduced two inverter microgrid with parameters $V_i = 250\sqrt{2}$ V, $P_i^* = 0$W, $\omega^* = 2\pi 50$rad/s, $f = 10$Hz and $\mathbf{L}_c = [1\ -1; -1\ 1]$.

4 Simulations

To validate our proposal, we simulated the network shown in Figure 1. Power sharing deviation for various droop coefficients and clock mismatches is demonstrated in Figure 2. As shown in Figure 2 (a) small droop coefficients and large drifts cause large power sharing error. Although the power sharing error is small with smaller drifts as shown in Figure 2 (c), it still exists. With the help of modified frequency droop, the power sharing error of any magnitude can be corrected in quick time as shown in Figure 2 (b,d).

According to condition (13) any value of $0 < k < 5$ will achieve stability and equal power sharing for the given network. Hopf bifurcation behaviour is shown when $k = 5$ and the system is rendered unstable for any values of $k > 5$. This is shown in Figure 3 using the frequency difference, $(\omega_1 - \omega_2)$.

5 Conclusion and future work

We have shown that power sharing in droop controlled inverters is very sensitive to uncertainty in frequencies

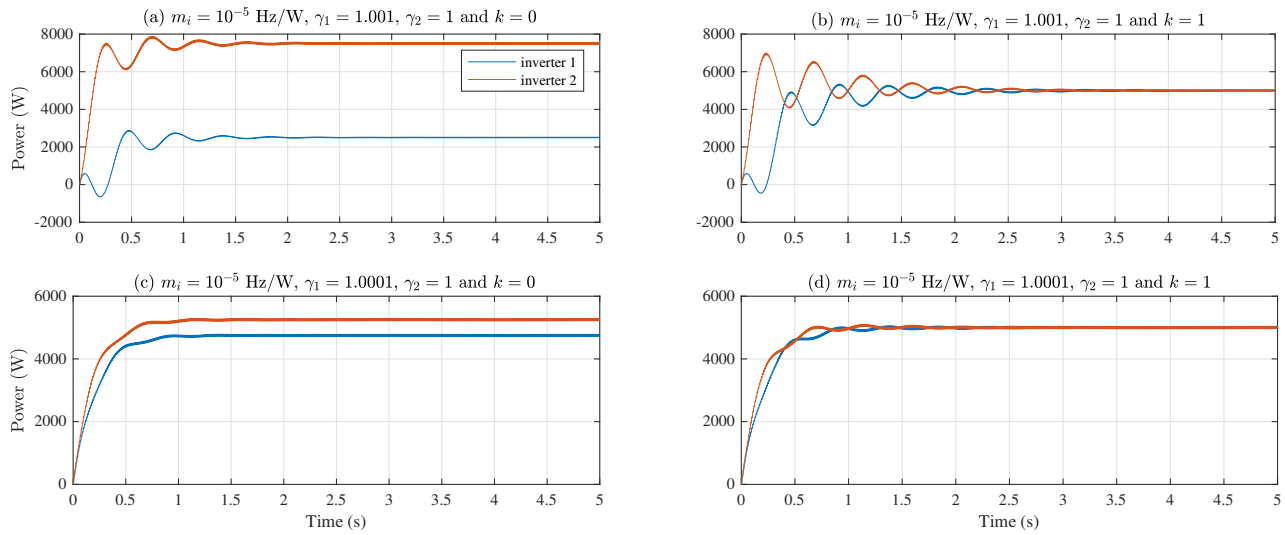

Fig. 2. Power sharing deviation in frequency droop controlled microgrid as a result of clock drift (a) $m_i = 10^{-5}$Hz/W, $\gamma_1 = 1.001$ and $\gamma_2 = 1$; and (c) $m_i = 10^{-5}$Hz/W, $\gamma_1 = 1.0001$ and $\gamma_2 = 1$. Power sharing correction using modified frequency droop (b) $m_i = 10^{-5}$Hz/W, $\gamma_1 = 1.001$ and $\gamma_2 = 1$ with gain $k = 1$; and (d) $m_i = 10^{-5}$Hz/W, $\gamma_1 = 1.0001$ and $\gamma_2 = 1$ with gain $k = 1$.

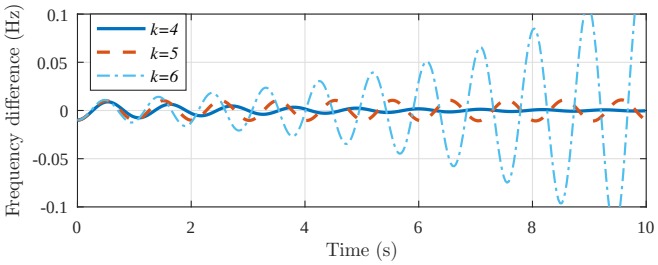

Fig. 3. Frequency difference, $(\omega_1 - \omega_2)$ between inverters for various values of k at $m_i = 10^{-6}$ Hz/W, $\gamma_1 = 1$ and $\gamma_2 = 0.9998$.

that might arise from clock drifts. We proposed a modified frequency droop controller which is based on internode communications. It has been shown that the control design introduced as supplementary to droop control can provide better steady state performance. Conditions are derived to guarantee in the presence of the proposed controller. Our control technique is robust to measurement uncertainties since there are no extra measurements involved. Standard secondary frequency control techniques may under-perform in the presence of clock drifts. Analysis and design of secondary frequency controllers that are robust to clock drifts will be addressed in future research. Although we have not considered communication delays and voltage amplitude mismatches in this work we appreciate their relevance and aim to address them in our future research.

6 Acknowledgement

The authors thank the anonymous reviewers for their invaluable comments and suggestions.

References

[1] M. Chandorkar, D. Divan, and R. Adapa, "Control of parallel connected inverters in standalone ac supply systems," *Industry Applications, IEEE Transactions on*, vol. 29, no. 1, pp. 136–143, Jan 1993.

[2] J. W. Simpson-Porco, F. Dorfler, and F. Bullo, "Synchronization and power sharing for droop-controlled inverters in islanded microgrids," *Automatica*, vol. 49, no. 9, pp. 2603 – 2611, 2013.

[3] J. Guerrero, L. Garcia de Vicuna, J. Matas, M. Castilla, and J. Miret, "A wireless controller to enhance dynamic performance of parallel inverters in distributed generation systems," *Power Electronics, IEEE Transactions on*, vol. 19, no. 5, pp. 1205–1213, Sept 2004.

[4] Q.-C. Zhong, "Robust droop controller for accurate proportional load sharing among inverters operated in parallel," *Industrial Electronics, IEEE Transactions on*, vol. 60, no. 4, pp. 1281–1290, April 2013.

[5] B. Shoeiby, D. Holmes, B. McGrath, and R. Davoodnezhad, "Dynamics of droop-controlled microgrids with unequal droop response times," in *Power Engineering Conference (AUPEC), 2013 Australasian Universities*, Sept 2013, pp. 1–6.

[6] T. Vandoorn, B. Renders, B. Meersman, L. Degroote, and L. Vandevelde, "Reactive power sharing in an islanded microgrid," in *Universities Power Engineering Conference (UPEC), 2010 45th International*, Aug 2010, pp. 1–6.

[7] J. Schiffer, R. Ortega, C. A. Hans, and J. Raisch, "Droop-controlled inverter-based microgrids are robust to clock drifts," in *American Control Conference (ACC)*, June 2015, pp. 2341–2346.

[8] L.-Y. Lu and C.-C. Chu, "Robust consensus-based droop control for multiple power converters in isolated micro-grids," in *Circuits and Systems (ISCAS), 2014 IEEE International Symposium on*, June 2014, pp. 1820–1823.

[9] C.-Y. Chang and W. Zhang, "Distributed control of inverter-based lossy microgrids for power sharing and frequency

regulation under voltage constraints," *Automatica*, vol. 66, pp. 85 – 95, 2016. [Online]. Available: http://www.sciencedirect.com/science/article/pii/S0005109815005464

[10] R. Olfati-Saber, J. Fax, and R. Murray, "Consensus and cooperation in networked multi-agent systems," *Proceedings of the IEEE*, vol. 95, no. 1, pp. 215–233, Jan 2007.

[11] Schneider Electric, "Conext XW inverter/charger product manual," 2014, [Online; accessed 8-November-2014]. [Online]. Available: http://www.schneider-electric.com/products/au

[12] Emmerson Network Power, "Chloride CP-70i 01 DC/AC inverter datasheet," http://www.emersonnetworkpower.com/documentation/en-us/products/industrialpower/documents/cp-70i/chloride%20cp-70i%2001%20dc-ac%20inverter_dsuk_rev3-062013.pdf, 2014, [Online; last accessed 14-June-2016].

[13] Magnum Dimensions, "The MSH-RE Series Inverter / Charger," http://www.magnum-dimensions.com/sites/default/files/manuals/spec/MSH-RE_series_datasheet_revB_%2364-0498_web.pdf, 2014, [Online; last accessed 14-June-2016].

[14] Power Stream, "Rugged, heavy duty and industrial grade 3-phase pure sine wave DC/AC inverters," http://www.powerstream.com/inverter-3-phase-24vdc-208vac-6000w.htm, 2016, [Online; last accessed 14-June-2016].

[15] Yueqing Sandi Electric Co., Ltd, "Solar Sine Wave Inverter," https://www.evworks.com.au/assets/files/Manual%20of%20SDP-10KW%20inverter.pdf, [Online; last accessed 14-June-2016].

[16] A. Bergen and D. Hill, "A structure preserving model for power system stability analysis," *Power Apparatus and Systems, IEEE Transactions on*, vol. PAS-100, no. 1, pp. 25–35, Jan 1981.

[17] N. Pogaku, M. Prodanovic, and T. Green, "Modeling, analysis and testing of autonomous operation of an inverter-based microgrid," *Power Electronics, IEEE Transactions on*, vol. 22, no. 2, pp. 613–625, March 2007.

[18] P. Kundur, N. Balu, and M. Lauby, *Power system stability and control*, ser. EPRI power system engineering series. McGraw-Hill, 1994.

[19] M. Andreasson, H. Sandberg, D. Dimarogonas, and K. Johansson, "Distributed integral action: Stability analysis and frequency control of power systems," in *Decision and Control (CDC), 2012 IEEE 51st Annual Conference on*, Dec 2012, pp. 2077–2083.

[20] J. Schiffer, D. Goldin, J. Raisch, and T. Sezi, "Synchronization of droop-controlled microgrids with distributed rotational and electronic generation," in *IEEE 52nd Annual Conference on Decision and Control (CDC)*, Dec. 2013, pp. 2334–2339.

[21] J. Schiffer, A. Anta, T. D. Trung, J. Raisch, and T. Sezi, "On power sharing and stability in autonomous inverter-based microgrids," in *IEEE 51st Annual Conference on Decision and Control (CDC)*, dec. 2012, pp. 1105 –1110.

[22] J. R. Silvester, "Determinants of Block Matrices," http://www.ee.iisc.ac.in/new/people/faculty/prasantg/downloads/blocks.pdf, 2014, [Online; accessed 30-June-2016].

[23] J. Broida and S. Williamson, *A Comprehensive Introduction to Linear Algebra*, ser. Advanced Book Program. Addison-Wesley, 1989. [Online]. Available: https://books.google.com.au/books?id=eyMlAQAAIAAJ

Ramachandra Rao Kolluri has been a Ph.D. student in Electrical and Electronic Engineering at The University of Melbourne since 2013. He joined IBM Research as a post-doctoral researcher in 2017 and his interests include renewable energy integration in microgrids.

Iven Mareels is Professor of Electrical and Electronic Engineering, and Dean of the Melbourne School of Engineering at The University of Melbourne since 2008. He is an expert in the area of systems engineering.

Tansu Alpcan has been with The University of Melbourne, Australia, since October 2011 where he is currently an Associate Professor. His main research interests are distributed decision making, game theory, and control with applications to energy markets, smart grid, and demand response.

Marcus Brazil is an Associate Professor and Reader in the Department of Electrical and Electronic Engineering at The University of Melbourne. Currently, his main research interests are in Optimal Network Design with a variety of applications.

Julian de Hoog is a Research Scientist at IBM Research Australia, and an Honorary Research Fellow at the University of Melbourne. His current research interests are in the application of forecasting and optimisation methods to the optimal operation of energy storage systems.

Doreen Thomas is a Professor and Head of the Department of Mechanical Engineering at The University of Melbourne. Her research interests are in network optimisation to applications in a range of areas including power networks and sensor networks.